Published in final edited form as:

Cell. 2018 January 11; 172(1-2): 305–317.e10. doi:10.1016/j.cell.2017.12.023.

Transmembrane pickets connect cyto-and pericellular-skeletons forming barriers to receptor engagement

Spencer A. Freeman[1], **Anthony Vega**[2], **Magdalena Riedl**[1], **Richard F. Collins**[1], **Phillip P. Ostrowski**[1], **Elliot C. Woods**[3], **Carolyn R. Bertozzi**[3], **Markku I. Tammi**[4], **Diane S. Lidke**[5], **Pauline Johnson**[6], **Satyajit Mayor**[7], **Khuloud Jaqaman**[2], and **Sergio Grinstein**[1,8]

[1]Program in Cell Biology, Peter Gilgan Centre for Research and Learning, Hospital for Sick Children, 686 Bay Street, 19-9800, Toronto, ON, M5G 0A4, Canada [2]Department of Biophysics, University of Texas Southwestern Medical Center, Dallas, TX, 75390, USA [3]Departments of Chemistry, and Molecular Biology, and Howard Hughes Medical Institute, University of California, Berkeley, California 94720, USA [4]Institute of Biomedicine, University of Eastern Finland, Kuopio, 70210, Finland [5]Department of Pathology, Cancer Research Facility, School of Medicine, University of New Mexico, Room 203, Albuquerque, NM, 87131, USA [6]Department of Microbiology and Immunology, University of British Columbia, Vancouver, British Columbia, Canada V6T 1Z3 [7]Cellular Organization and Signaling, National Centre for Biological Science, Tata Institute for Fundamental Research, Bangalore 560 065, India [8]Keenan Research Centre of the Li Ka Shing Knowledge Institute, St. Michael's Hospital, 290 Victoria Street, Toronto, ON, Canada, M5C 1N8

SUMMARY

Phagocytic receptors must diffuse laterally to become activated upon clustering by multivalent targets. Receptor diffusion, however, can be obstructed by transmembrane proteins ("pickets") that are immobilized by interacting with the cortical cytoskeleton. The molecular identity of these pickets and their role in phagocytosis have not been defined. We used single-molecule tracking to study the interaction between Fcγ receptors and CD44, an abundant transmembrane protein capable of indirect association with F-actin, hence likely to serve as a picket. CD44 tethers reversibly to formin-induced actin filaments, curtailing receptor diffusion. Such linear filaments predominate in the trailing end of polarized macrophages, where receptor mobility was minimal. Conversely, receptors were most mobile at the leading edge, where Arp2/3-driven actin branching predominates. CD44 binds hyaluronan, anchoring a pericellular coat that also limits receptor displacement and obstructs access to phagocytic targets. Force must be applied to traverse the pericellular barrier, enabling receptors to engage their targets.

Correspondence should be addressed to Sergio Grinstein (sergio.grinstein@sickkids.ca).

AUTHOR CONTRIBUTIONS

S.F. conducted experiments. M.R. conducted biochemical assays. A.V. and K.J. wrote the DCMSS and performed SPT analyses. P.O. performed STED microscopy. R.C., E.W., C.B., M.T., D.L., P.J., and S.M made and provided reagents. S.F. and S.G. designed the study and wrote the manuscript with input from all authors.

Graphical abstract

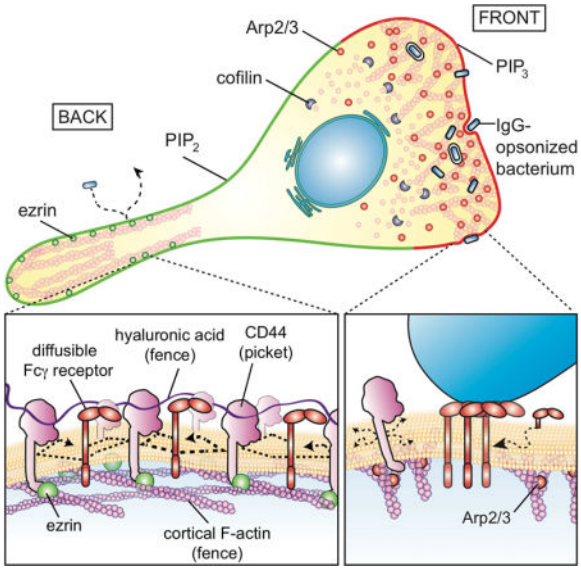

Immunoreceptors, like those responsible for triggering phagocytosis, are activated by homo oligomerization, induced by exposure to multivalent ligands. Such clustering involves lateral displacement of the receptors in the plane of the membrane. The presentation of stimuli, such as motile bacteria that must be captured and eliminated by phagocytes, is often transient. Thus, opportune receptor oligomerization and activation must occur rapidly. To this end, fast, unimpeded lateral diffusion of receptors would be advantageous. However, contrary to the predictions made by the fluid mosaic model of Singer and Nicolson (1972), plasmalemmal proteins do not diffuse freely in membranes (Kusumi et al., 2012). Instead, they often appear confined, displaying diffusion coefficients that are orders of magnitude lower than in pure lipid bilayers. Such observations led Kusumi et al. to postulate the existence of diffusion barriers, cytoskeletal fences affixed to the plasmalemma by transmembrane protein pickets (Kalay et al., 2014; Kusumi et al., 2012; Morone et al., 2006).

The limited lateral mobility applies also to GPI-linked proteins that are anchored to the exofacial leaflet of the membrane (Saha et al., 2015) and, to a lesser extent, to lipids of the outer leaflet; such molecules are not in contact with cytoskeletal components. It would therefore appear as if barriers to diffusion exist within and/or beyond the lipid bilayer. Conceivably, transmembrane and extracellular portions of the immobile pickets, together with any adherent components, could account for the restricted mobility of lipids and lipid-anchored proteins (Trimble and Grinstein, 2015).

While the notion of transmembrane pickets has been discussed widely and is generally acknowledged (Nakada et al., 2003), the molecular identity and behavior of such entities remain largely unknown. To serve as *bona fide* pickets –i.e. to be of functional consequence to the behavior of diffusing bystanders– transmembrane proteins have to be: a) of high abundance, and b) immobilized by the submembrane skeleton, at least temporarily. Based on

these features, we hypothesized that CD44 might serve as a key picket in immune cells, where it is highly expressed. CD44 is a single-spanning transmembrane protein that links to the cortical skeleton via ezrin and ankyrin, which in turn associate with actin and spectrin, respectively. CD44 is also endowed with an extracellular Link domain capable of binding hyaluronan, potentially linking the picket fence to a pericellular coat that may itself alter protein diffusion. We used single-particle tracking, molecular and pharmacological manipulations to characterize the association of CD44 with the cytoskeleton and the resulting effects on the mobility of phagocytic receptors. In addition, we analyzed its role in the generation of a pericellular matrix –akin to an exoskeleton– that shields the cell surface, curtailing not only receptor mobility but also the access of phagocytic targets.

RESULTS

Tethering to the submembrane actin cytoskeleton mediates “stop-and-go” diffusion of CD44

For transmembrane molecules that attach to the cytoskeleton (i.e. “pickets”) to significantly alter the ability of bystander molecules to diffuse, they must be present at high density. To determine the abundance of CD44, we produced Fab fragments from a monoclonal antibody (IM7) against the ectodomain of CD44 and conjugated them with biotin. The number of Fabs bound to the surface of bone marrow-derived macrophages (BMDM) under saturating conditions was determined by comparison with known quantities of Fab, using avidin-peroxidase (Figure 1A). Fab bound non-specifically was determined using BMDM from CD44 knockout ($CD44^{-/-}$) mice. On average, wildtype BMDM expressed $\approx 10^6$ copies of CD44/cell on their surface. Comparable numbers were found for primary human macrophages (Figure 1A).

CD44 can interact with cortical actin filaments via ezrin/radixin/moesin (ERM); its cytosolic tail can bind ERM that, in turn, possess an actin-binding domain (Fehon et al., 2010). This association was validated in macrophages by sedimenting the cytoskeleton following extraction with non-ionic detergent. A considerable fraction of CD44 co-sedimented with actin filaments (Figure 1A). In contrast, FcγIIA/B receptors (CD32), integral proteins that –like CD44– span the membrane once, but are not thought to associate with the cortical skeleton, were entirely soluble (Figure 1B). Sedimentation of CD44 depended on the integrity of the actin filaments, as it was eliminated by latrunculin A.

We used Fab fragments of specific antibodies to analyze the diffusive behavior of CD44, tracking single molecules on the surface of live BMDM with nanometer precision (Figure S1). At the density used (10 ng/mL), the Fab fragments labeled single CD44 molecules, as the modal fluorescence intensity of Cy3-conjugated anti-CD44 Fab fragments on the cell surface matched that of mono-dispersed Fabs attached to glass, and underwent single bleaching steps (Figure S1, Video 1). Perusal of the tracks generated by CD44 on the membrane revealed the existence of at least two distinct states: prolonged (seconds-long) periods of confinement or immobilization, punctuated by bursts of mobile behavior (Figure 1C–D; Videos 1–2).

In order to quantitatively characterize the clearly inhomogeneous motion of CD44, we devised a new transient motion analysis approach termed “divide-and-conquer moment scaling spectrum” analysis (DC-MSS). DC-MSS utilizes local movement descriptors throughout a trajectory to divide it into segments that are classified via MSS; the MSS analysis is then used to refine trajectory segmentation (see Methods). This allows for efficient identification of distinct mobility states along each trajectory. The DC-MSS analysis distinguished three different states: freely mobile (Brownian), confined-mobile, and tethered (immobile). In untreated macrophages CD44 was tethered >20% of the time, confined-mobile ≈50% of the time and free the rest of the time (Figure 1E). Fixation with paraformaldehyde (PFA) markedly increased the fraction of time in the tethered mode (to ≈80%), at the expense of the confined-mobile and freely mobile fractions (Figure 1E). Tethered molecules had an average confinement area of ≈0.005 μm^2, closely matching that of particles fixed by PFA (Figure 1F). This area was indistinguishable from the positional uncertainty inherent to the measurements, determined using fluorophores immobilized on glass. The confinement area of confined-mobile molecules was on average 3times larger than that of tethered molecules (Figure 1F). Importantly, tethering was almost eliminated by treatment with latrunculin (5 min), which also decreased the fraction of confined molecules, while greatly increasing Brownian motion (Figure 1C,E).

We performed experiments using direct conjugation of the Fab fragments with Cy3B or biotinylation of Fabs followed by labeling with avidin-coated quantum dots (Qdots). Essentially identical results were obtained with both approaches (*cf.* Figures 1 and S1). Because the dots are less susceptible to photobleaching and yield longer tracks, they were more suitable for DC-MSS analysis. Tracks obtained with Cy3B were shorter and, to minimize bleaching, were obtained using slower frame rates not adequate for DC-MSS analysis; for this reason the confined and tethered modalities were not differentiated when using Cy3B (e.g. Figures 1I and 3F).

The preceding data are consistent with the existence of CD44 in two interconvertible states: tethered to, and dissociated from the actin skeleton. The dissociated form can in turn exist within a confinement zone delimited by the skeleton (i.e. a “corral”), or move freely outside such restricted zones. While tethered, CD44 could serve as a picket. Tethering presumably results from the interaction of CD44 with ezrin and/or ankyrin, which in turn associate with the actin cytoskeleton. Consistent with this model, truncation of the cytosolic tail of CD44 (Figure 1G), which contains the ezrin-and ankyrin-binding motifs, greatly reduced tethering (Figure 1H) while increasing the diffusion coefficient (Figure 1J).

By affixing the actin skeleton to the cytosolic aspect of the membrane, pickets like CD44 could alter the mobility of other membrane proteins. The cytosolic domains of proteins such as phagocytic receptors could collide with the cytoskeletal mesh, confining them within corrals. However, the diffusion barrier could be posed by the transmembrane or ecto-domains of the pickets themselves. In this scenario, rather than the pickets serving to anchor the skeleton, the opposite effect may be more important, namely the immobilization of the pickets by their association to the underlying actin mesh. To test the relative contribution of the transmembrane and cytosolic domains of receptors to their mobility in the plane of the membrane, we compared the behavior of full-length and truncated forms of FcγRIIA

(lacking the cytosolic tail; Figure 1G), using Fab fragments directed to the extracellular domain. These receptors were expressed heterologously in COS-1 cells to avoid confounding effects of endogenous FcγRIIA/B. Unlike CD44, FcγRIIA showed only confined-mobile and freely mobile modes, but no discernible tethering. Importantly, truncation of the cytosolic tail had no significant effect on the mobility of the Fc receptors: neither the confinement area nor the diffusion coefficient were altered by deletion of the tail. The preceding findings suggest that Fc receptor confinement is caused by collisions of its transmembrane and/or extracellular domains with immobile pickets, and not by trapping of its cytosolic tail within corrals formed by the cortical cytoskeleton.

CD44 is a major picket in the macrophage plasma membrane

The preceding experiments indicate that CD44 can tether to the cortical skeleton and could potentially serve as a picket, but do not reveal its contribution to the mobility of other (bystander) molecules. This was explored by examining the spatial relationship between CD44 and FcγRIIA in human macrophages using stimulated emission depletion (STED) microscopy. STED imaging revealed networks of CD44 that corralled receptors, consistent with a picketing role for CD44 (Figure 2A). We then compared the behavior of Fcγ receptors in wildtype and $CD44^{-/-}$macrophages (Figure 2B,C), and in immortalized macrophages (RAW264.7 cells, termed RAW hereafter) where CD44 was expressed normally or knocked down by siRNA (Figure 2B,D). Fcγ receptors (CD16 and CD32) were probed together using Fab fragments of monoclonal antibody Clone 93 that recognizes both types. As shown in Figure 2C–D, the diffusion coefficient of the Fcγ receptors was considerably higher in macrophages where CD44 was absent (Figure 2B,C) or silenced (Figure 2B,D) than in control cells. As expected, the cytosolic domain of CD44 is required for it to curtail the diffusion of Fcγ receptors (Figure 2E).

To ascertain whether CD44 in fact curtails molecular motion by acting as a transmembrane/exofacial picket, we tracked the mobility of a lipid-anchored molecule. A synthetic probe was used for these tests: a rigid glycopolymer biotinylated at one end and acylated at the other, promoting its insertion into the outer leaflet of the membrane (Figure 2F). Attachment of Qdots to the terminal biotin enabled us to track the glycomimetic on the surface of wildtype and $CD44^{-/-}$macrophages. The probe was clearly less mobile in cells expressing CD44: the fraction of time that the glycopolymer was confined was greater and the diffusion coefficient lower in wildtype than in $CD44^{-/-}$cells (Figures 2G–I). Together, these results establish CD44 as a picket anchored to the cortical skeleton, capable of altering the behavior of diffusing bystander molecules.

The actin-binding domain of ezrin is sufficient to tether pickets to Rho/formin-generated actin filaments

Given the influence of CD44 pickets on bystander diffusion, we studied in greater depth the mechanisms that govern their tethering and release. We used an ezrin inhibitor to assess the contribution of ERM proteins to the tethering of CD44 to actin filaments. Treatment with the inhibitor caused detachment of CD44 from the actin skeleton, as indicated by sedimentation experiments (Figure 3A). Note that, unlike latrunculin (Figure 1B), the ezrin inhibitor did

not compromise the integrity of the skeleton, which sedimented normally following detergent extraction.

We next tested whether attachment to ERM proteins suffices to account for the tethering behavior of CD44. We generated a chimeric construct consisting of the actin-binding domain of ezrin, linked to the transmembrane domain of the Fc receptor tagged extracellularly with a hemagglutinin (HA) epitope (Figure 3B). Biotin-labeled anti-HA Fab fragments and avidin coupled Qdots were used to track this chimera. Strikingly, the exogenous chimeric construct mimicked closely the behavior of CD44, spending ≈20% of the time tethered (Figure 3C). Tethering was caused by binding of the ezrin domain to actin. This was concluded by tracking an analogous chimeric construct with a mutation (R579A) that precluded actin binding by the ezrinderived domain. The mutation greatly reduced tethering, while increasing the diffusion coefficient more than 3-fold (Figure 3C–D). We concluded that binding to ERM proteins is likely the dominant factor bestowing tethering properties to CD44.

This model predicts that the fraction of time that CD44 spends in the tethered mode should be proportional to the availability of suitably oriented actin filaments. Using inhibitors, we observed that formins contribute significantly to the maintenance of the cortical skeleton of monocytes, while Arp2/3-mediated nucleation is less important (Figure S2A). We therefore attempted to increase the availability of cortical actin filaments by stimulating formins using a Rho activator (CN03). Treatment with the activator caused a marked increase in submembranous actin (Figures 3E and S2B), which was accompanied by alteration in the motion type and diffusion coefficient of the transmembrane ezrin-domain chimera. Tethering and confinement, assessed jointly using Cy3B, increased considerably, as the fraction of freely mobile chimera decreased (Figure 3F). As a result, the overall diffusion coefficient dropped from $0.048 \pm 0.009\ \mu m^2\ s^{-1}$ to $0.028 \pm 0.006\ \mu m^2 s^{-1}$ (means ± S.E of >25 determinations). Notably, inhibition of Arp2/3 using CK666 was without effect, suggesting little interaction between Arp2/3-branched actin networks and the actin-binding domain of ezrin (Figure 3F). The diffusion of endogenous CD44 paralleled these effects (Figure 3G), lending confidence to comparisons between the synthetic and CD44 pickets. Moreover, activation of the Rho/formin axis also reduced the diffusion coefficient of the Fcγ receptors (Figure 3H), ostensibly because of increased tethering of pickets like CD44. As before, alteration of Arp2/3 activity was without effect on receptor mobility.

The intermittent untethering of pickets is stimulated by actin-severing proteins

Despite containing an exposed actin-binding domain, the chimeric synthetic pickets still underwent periodic exits from the tethered state (Figure 3C). This may reflect the intrinsic tendency of the ezrin domain to dissociate from actin filaments, but could also indicate that the filamentous mesh that underpins tethering is unstable. To test the latter possibility we reduced the rate at which actin filaments are severed. This was accomplished by expressing a dominant-negative form of Slingshot (SSH-1L), the phosphatase responsible for the dephosphorylation and hence activation of cofilin, a key F-actin-severing protein (Figure 3I). Expression of the mutant form of SSH-1L greatly increased the density of cortical F-actin and, like the stimulation of Rho/formins, caused cell rounding (Figure S2C). The increase in

F-actin density was accompanied by an increase in CD44 tethering (Figure 3J), consistent with the notion that remodeling (e.g. severing) of the cortical skeleton limits the fraction of time that CD44 is immobilized.

Polarized cytoskeletal networks orchestrate picket stabilization and receptor diffusion

Chemoattractants guide immune cells to sites of infection. During vectorial migration, cytoskeletal networks polarize generating distinct leading and trailing regions; upon arrival to their destination, phagocytes engulf the infecting organisms. Phagocytosis occurs at the leading edge of the polarized cell, making the process efficient. At the front of migrating cells, actin severing, turnover and branching are fuelled by cofilin that is locally activated to drive cell “steering” (Ghosh et al., 2004). At the back, myosin-driven contraction favors the retraction of the tail or uropod (Lammermann et al., 2008; Lomakin et al., 2015); in lymphocytes the uropod is rich in ezrin (Serrador et al., 1998). A similar polarization of ezrin in macrophages would potentially result in unequal tethering of CD44 at the front and back of the cells. This possibility was analyzed by immunostaining. As shown in Figure 4A, ezrin is indeed enriched at the back of polarized macrophages, despite similar F-actin density at both ends of the cell.

Knowing that ERM proteins influence the mobility of pickets and bystander molecules, and in view of the unequal distribution of ezrin in polarized macrophages, we performed single-particle tracking at the front and back of such cells (Figure 4B). A striking difference in the mobility of the Fcγ receptors was observed: while most of them moved freely in the front of the cell, the majority were confined at the back (Figures 4B and C). The overall diffusion coefficient was considerably greater at the front (Figure 4D). Based on our earlier conclusions, this differential behavior is at least partly due to unequal tethering of pickets at both ends of the cell. Indeed, CD44 was also predominantly free near the leading edge, but mostly tethered/confined at the back (Figure 4E), and the diffusion coefficient was several-fold higher at the front than in the uropod (Figure 4F).

The low affinity of Fcγ receptors requires the formation of high-avidity multimeric clusters to properly secure phagocytic targets; this in turn requires coalescence of diffusing receptors when cells are exposed to multivalent ligands. A corollary of the observed polarity-dependent differences in mobility is that receptors at the front of the cell would bind IgG-opsonized prey more efficiently. This premise was tested experimentally by exposing polarized macrophages to IgG-coated *Salmonella.* Bacteria bound almost exclusively to the front of the cells, with very few attaching to the back (Figure 4G). When the number of bacteria were counted and normalized per unit area, the front quartile of the cells bound 0.0054 ± 0.0016 bacteria/μm^2, while only 0.0006 ± 0.0011 bacteria/μm^2 bound at the back, nearly a ten-fold difference.

To assess if depleting F-actin networks that tether CD44 at the back of cells was sufficient to increase particle binding, polarized macrophages were treated with the Rho inhibitor, TAT-C3. Inhibiting Rho increased the diffusion of CD44 pickets and Fc receptors (Figure 4H–I), and also resulted in a gross morphological change to the cells, which spread radially and adhered extensively to the coverslip (not shown). To avoid the confounding effects of unequal surface area exposure, we instead assessed the effect of TAT-C3 on target binding in

suspended macrophages, where a Rho/formin-derived actin cytoskeleton predominates (Figure S2). Remarkably, suspended –but otherwise untreated– macrophages rarely bound phagocytic targets (Figure 4J–K). The diminished binding was at least partly attributed to the dense cortical actin cytoskeleton, as cells where Rho was inhibited were better able to engage particles. Conversely, increasing the cortical actin density by activating Rho with CN03 curtailed signaling responses when suspended cells were allowed to sediment onto micro-patterned IgG (Figure S3B–C), and reduced the phagocytic efficiency (Figure S3D). These results are consistent with the notion that the Rho/formin-derived actin networks that tether CD44 oppose the engagement, and ultimately the engulfment of phagocytic targets.

Pericellular hyaluronan serves as an exoskeletal fence that restricts receptor diffusion

In addition to the cytosolic motifs that associate with ezrin and ankyrin, CD44 also possesses an extracellular Link domain that can bind the glycosaminoglycan (GAG) hyaluronan (HA) (Aruffo et al., 1990), a long, unbranched polymer. Macrophages express HA synthases (Chang et al., 2014) and are also capable of binding exogenous HA, a major component of the extracellular matrix; CD44 is mostly responsible for the binding (Lee-Sayer et al., 2015). We therefore analyzed the possible contribution of HA to the distribution and mobility of CD44. BMDMs grown in isolation had appreciable HA on their surface, that could be detected by ELISA (Figure 5A) and visualized using a fluorescent HA-binding protein (Figure 5B). The HA was virtually eliminated by treating the macrophages with hyaluronidase (HAase). That CD44 is the main receptor for HA on the surface of macrophages was deduced by comparing the amount of HA associated with the membrane of BMDMs from wildtype and $CD44^{-/-}$mice (Figure 5B).

Given their length [estimated to reach several microns; (Laurent and Fraser, 1992)], we theorized that strands of HA could bridge adjoining CD44 molecules, potentially contributing to their tethering and/or generating an exofacial fence. This would require the HA strands to be immobilized. We assessed the mobility of HA on the surface of the cells using a biotinylated HA-binding protein and streptavidin-conjugated Qdots. HA was found to be largely immobile (Figure 5C), with a mean diffusion coefficient of only 0.0057 $\mu m^2 s^{-1}$. The majority (77.4%) of the features detected were restricted within a confinement radius of just 61 nm. If sufficiently dense, this immobile HA mesh could constrain the diffusion of bystanding molecules. This was tested by measuring the effects of HAase on the behavior of the lipid-anchored glycopolymer described above. As illustrated in Figure 5D–E, enzymatic degradation of HA decreased the confinement of the glycopolymer, while increasing its diffusion coefficient. Importantly, degradation of HA had a similar effect on the diffusion of Fc receptors and CD44 itself (Figure S4C–D).

We also removed HA from the surface of macrophages, seeded them onto coverslips coated with HA, and measured the diffusion of Fc receptors along the ventral membrane, i.e. the surface that contacted the coverslips. These experiments demonstrated that the presence of immobilized HA sufficed to restrain the diffusion of Fc receptors in wildtype, but not $CD44^{-/-}$macrophages (Figure 5F).

To further analyze the ability of the pericellular coat to restrict the mobility of transmembrane proteins, we induced the formation of a rich HA coat by transfecting HA

synthase 3 (HAS3) into COS-1 cells stably expressing FcγRIIA receptor. As described (Kultti et al., 2006), expression of HAS3-GFP induced the formation of a thick HA coat (Figure 6A). The HA generated by the ectopic expression of HAS3-GFP caused a marked change in the mobility of Fcγ receptors, increasing their confinement (Figure 5G), which reduced their diffusion coefficient by more than 40% (Figure 5H). These results suggest that HA bound to membrane receptors, e.g. CD44, influences the mobility of membrane-associated molecules. This effect is exerted by further immobilizing transmembrane pickets and/or by generating a pericellular mesh that impedes diffusion in the plane of the membrane (Figure 5I). Of note, HA can produce these effects whether it is directly bound to the plasma membrane or acting in *trans* (i.e. as part of a stationary surface that the macrophage interacts with).

Pericellular hyaluronan restricts access to phagocytic receptors

The effectiveness of the heterologous expression of HAS3-GFP was validated using bright-field microscopy, as described (Kultti et al., 2006). This approach is based on the formation of a dense glycocalyx coat surrounding the HA-expressing cells, which excludes red blood cells deposited on top of the transfectants (Figure 6A). Clearly, pericellular HA can limit the access of particles to the cell surface; this could have important implications for phagocytosis considering that the majority of phagocytic receptors, including FcγR, only extend short (≈5 nm) distances from the plasmalemmal bilayer. To substantiate this notion we compared the phagocytic efficiency of cells that were, or were not transfected with HAS3-GFP. Despite expressing comparable levels of Fcγ receptors (Figure 6C), COS-1 cells expressing HAS3-GFP bound and internalized phagocytic targets very poorly, six-fold less than their untransfected counterparts (Figure 6B).

Barriers to phagocytic receptor access are overcome by force

How do phagocytic targets overcome the glycocalyx to engage receptors in the first place? It is conceivable that the pericellular coat is discontinuous, displaying openings where contact with the receptors can occur. This possibility was explored analyzing the distribution of the HA coat around the membrane of professional phagocytes. Remarkably, in adherent polarized cells membrane protrusions where the binding of phagocytic targets is normally initiated were largely devoid of endogenous pericellular HA (Figure S4A). These observations suggest that the glycocalyx can be displaced from defined regions of the membrane by dynamic actin remodeling, thus facilitating particle access. Accordingly, overexpression of HAS3-GFP in these cells produced a richer, more homogeneous coat of HA (Figure S4B) that impaired their ability to bind and ingest targets (Figure 6D and S4E).

Centrifugation of particles onto macrophages is routinely used to enhance phagocytic efficiency. We therefore hypothesized that in addition to heterogeneity in the distribution of HA, mechanical force exerted either by the approaching particle and/or by the phagocyte itself may displace the glycocalyx laterally, bringing phagocytic ligands in close apposition with their receptors. We used wheat germ agglutinin (WGA) as a marker of the glycocalyx to evaluate this possibility. To assess whether extrinsic mechanical force could mediate the displacement of the glycocalyx, we first disabled the actin cytoskeleton using latrunculin to eliminate the uncontrolled extension of protrusions from the macrophage. Next, we allowed

latex beads to settle on the surface of the cells. The gravitational force exerted by 5 μm latex beads induced only modest exclusion of WGA from a small area of the membrane (Figure 7A). We then used centrifugation to apply perpendicular force on the membrane at the junction with the bead. Strikingly, this sufficed to exclude WGA from the contact area (Figure 7A). The degree of exclusion was proportional to the force applied. To further assess the contribution of mechanical force to phagocytosis, we used small particles of moderate density (e.g. 1.5 μm latex beads, coated with IgG), which can only apply weak force on the membrane and do not displace the glycocalyx effectively. As a result, they bind poorly to the receptors on the surface of macrophages. However, binding was increased many-fold by applying centrifugal force (Figure 7B).

In the preceding examples, force was applied to the membrane of the phagocyte by artificial means (i.e. centrifugation). However, it can also be effected by motile targets, such as flagellated bacteria. This is illustrated in Figure 7C, where *Salmonella* coated with an antibody targeted to the cell wall (anti-O) were promptly bound by the macrophages. In contrast, *Salmonella* opsonized with an antibody to the flagella (anti-H) bound very poorly to the cells. As shown in Video 3, binding of the antibody to the flagella paralyzes the bacteria, which are no longer able to penetrate the glycocalyx to reach the phagocytic receptors.

That the glycocalyx is the barrier that hinders access to the membrane was emphasized by overexpression of HAS3. In such cells, even large (8 μm) beads that normally have enough momentum to cross the pericellular coat, had difficulty reaching the surface receptors (Figure 7D). Application of additional force (500 xg) drove the beads across the thickened glycocalyx, restoring binding.

These results are consistent with the need for force to traverse a pericellular coat that is anchored to membrane pickets. This notion was validated comparing wild-type and $CD44^{-/-}$ macrophages (Figures 7E–F). The small (1.5 μm) opsonized beads that associated poorly to normal macrophages were bound much more effectively by CD44-deficient cells. As predicted, this difference was minimized when centrifugal force enabled the particles to enter the more rigid glycocalyx of wild-type cells. Similarly, immobile (anti-H opsonized) bacteria bound more readily to $CD44^{-/-}$macrophages, a difference that was not significant in the case of motile (anti-O opsonized) *Salmonella* (Figure 7E).

Because CD44 attaches to the cytoskeleton and the degree of tethering was shown above to be proportional to the abundance and stability of actin filaments, we predicted that increasing Rho activity would translate into a less penetrable pericellular coat and a more stable picket fence that would curtail the lateral displacement of phagocytic receptors. These predictions were tested experimentally by treating the cells with a Rho activator or by inhibiting Slingshot. Stimulating Rho activity with CN03 greatly depressed the ability of IgG-opsonized particles to bind to the surface of the macrophages, an effect that was partially overcome by the application of perpendicular (centrifugal) force (Figure 7G). Similarly, dominant-negative slingshot impaired binding, while overexpression of the wildtype phosphatase improved it modestly. As before, force overcame the inhibition of the phosphatase (Figure 7H).

DISCUSSION

The “picket-fence” model was conceptualized more than 20 years ago to account for the seemingly aberrant diffusion of plasmalemmal proteins (Kusumi and Sako, 1996). However, definitive identification of *bona fide* pickets has been elusive. We chose to investigate CD44 as a potential picket attaching the cortical actin fence to the plasma membrane because of its abundance ($\approx 10^6$ copies/cell) and documented association with ezrin and ankyrin. Our data indicate that CD44 is a significant contributor to the barrier that limits the diffusion of other (bystander) molecules in the plane of the membrane, an effect that is magnified by its ability to associate with the pericellular HA coat. While clearly important, CD44 is by no means the only picket: macrophages also express other transmembrane proteins that link to the actin cytoskeleton via ERM proteins, including CD43 and ICAM. In addition, pickets may bind the cytoskeleton using other adaptors (e.g. NHERFs, or talin in the case of integrins) or do so directly.

Kusumi et al. originally envisioned the pickets as being stably attached to a rigid, immutable cytoskeleton, generating rather permanent partitions (corrals) that diffusible molecules had to escape (“hop”) in order to traverse longer distances (Fujiwara et al, 2002). Our findings depart from this model in two notable respects: first, the pickets need not be permanently attached to the cytoskeletal fence. Transmembrane proteins such as CD44, CFTR (Haggie et al., 2006) and CBP (Chen et al., 2009) associate with cortical actin via reversible interactions, resulting in intermittent tethering punctuated by diffusion within and across cytoskeletal corrals. Secondly, the stability of the cytoskeletal mesh that generates the diffusion-limiting corrals can vary greatly: while the membrane skeleton of red cells is relatively stable, forming a uniform quasi-hexagonal network, the cortical skeleton of nucleated cells can be much more dynamic. The myeloid cells used in our studies, which continuously remodel their cytoskeleton to survey their environment, may be an extreme example. Moreover, cytoskeletal structure –and hence stability– vary not only among cells, but also within different regions of individual cells (e.g. the soma vs. dendrites and axon of neurons, or the apical vs. basolateral membranes of epithelial cells), but also according to their functional state. Thus, acute cytoskeletal remodeling occurs during cell migration or spreading, cytokinesis, and tissue morphogenesis.

Our results also indicate that not all actin assemblies support tethering equally. CD44 tethers preferentially to actin filaments polymerized in response to Rho GTPases, and not Arp2/3branched networks. Rho binds to formins that add actin subunits to growing, linear filaments in a processive manner. Why do pickets prefer linear rather than branched actin? One possibility is that the orientation of the filament network vis-à-vis the membrane governs binding. Linear actin polymers that run parallel to the plasma membrane may provide latches onto which ezrin grasps. Branched networks, on the other hand, tend to orient perpendicularly to the membrane in order to generate membrane protrusions. Interestingly, we found that leukocytes in circulation, which are quiescent, have a dense cortical actin cytoskeleton polymerized by formins. As these cells cross the endothelium and enter tissues they become elaborately ruffled via actin branching and severing. Such actin remodeling would disengage pickets, causing receptors to diffuse more rapidly, priming the cells for encounters with foreign particulates.

Linear and branched actin networks coexist in cells, but are not necessarily distributed equally. A prime example is presented by cells performing chemotaxis, where branching occurs predominantly at the leading edge, while myosin-based contractility of linear actin bundles occurs at the rear. The asymmetric distribution of plasmalemmal phosphoinositides supports the polarization of the distinct actin networks: at the back, PtdIns(4,5)P_2 recruits ERM and cofilin, fostering anchorage and stabilization of linear filaments. At the front PtdIns(3,4,5)P_3 recruits GEFs that activate Rac to nucleate branched actin via Arp2/3. This dichotomy relies on the maintenance of front-to-back gradients of the phosphoinositides. We propose that pickets like CD44 contribute to the maintenance of such gradients, providing a positive feedback to the polarization machinery. By recruiting ERM and stabilizing the meshwork, PtdIns(4,5)P_2 would immobilize pickets that would, in turn, constrain phospholipid redistribution. In support of this idea, depletion of PtdIns(4,5)P_2 by activating phospholipases with a calcium ionophore led to increased picket diffusion (Figure S5A–B). In addition, generating PtdIns(3,4,5)P_3 by treating the cells with LPS similarly increased the mobility of CD44 and of phagocytic receptors (Figure S5C–D). As a consequence, LPS enhanced phagocytic efficiency (Figure S5E).

While pickets restrain and shield receptors at the cells' trailing edge, their rapid diffusion near the front favors binding of target particles to this region. Thus, the various chemoattractants that emanate from sites of infection would not only direct the leukocytes but, by polarizing the cytoskeleton, would also polarize and augment their phagocytic efficiency upon arrival. The inactivation of ERMs and release of pickets also decreases membrane tension (Faure et al., 2004), allowing for changes in cell shape, including the formation of phagocytic cups. It is befitting to speculate that phosphoinositides play a role in this context as well, inasmuch as PtdIns(3,4,5)P_3 has been implicated in alleviating membrane tension during phagocytosis (Masters et al., 2013).

In addition to serving as a picket, CD44 maintains HA strands on the cell surface. Its single Link domain binds HA weakly (Lesley et al., 2000) and therefore transiently, but the cooperative effect of myriad CD44 molecules ensures that the long HA strands are firmly retained on the cell surface. The resulting intricate exofacial mesh, together with other components of the glycocalyx, pose a physical obstacle to the approach of particles, potential phagocytic targets. Such a barrier is significant and must be overcome to enable productive contacts with phagocytic receptors. Application of force, whether by the particle or by the phagocytic cell, can accomplish this goal. We speculate that, when activated by inflammatory stimuli, macrophages extend branched actin-driven protrusions to scan for intruders. Such protrusions exert outward force and, in addition, create areas of reduced exoskeletal resistance and increased receptor mobility. Indeed, the glycocalyx formed by hyaluronan is virtually absent in the front edge of some migrating cells (Pienimäki et al. 2001) and also in polarized macrophages (Figure S4). This convergence of events is optimal for target engagement. Additionally, low affinity receptors (e.g. some classes of scavenger receptors) may extend beyond the glycocalyx to make first contact with phagocytic prey, luring them to the relatively short, more effective receptors, like FcγR.

In summary, we have demonstrated the existence of tethered transmembrane proteins (pickets) in immune cells that curtail phagocytic receptor engagement in two ways: 1) by

forming physical barriers, they limit the lateral diffusion of the receptors and 2) they anchor GAGs to the surface, stabilizing a pericellular coat or exoskeleton that limits the access of particulates to the receptors. The shielding effect by pickets, which is inhomogeneous in different domains of migrating cells, prioritizes binding to those regions most likely to encounter relevant targets. Lastly, it is worth emphasizing that the picket fence is fluid, constantly undergoing remodeling either because of reversible detachment of the pickets from the cytoskeletal mesh, or as a result of severing and formation of the latter.

STAR METHODS

CONTACT FOR REAGENT AND RESOURCE SHARING

Further information and requests for resources and reagents should be directed to and will be fulfilled by the Lead Contact, Sergio Grinstein (sergio.grinstein@sickkids.ca)

EXPERIMENTAL MODEL AND SUBJECT DETAILS

Cell isolation and culture—Primary murine macrophages, were derived from the marrow of femoral bones from 6–8 week old female C57Bl/6 wildtype or $CD44^{-/-}$mice (The Jackson Laboratory). Cells were washed before culturing in DMEM with L-glutamine containing 10% heat-inactivated fetal calf serum and 100 U/mL penicillin and 100 μg/mL streptomycin. MCSF was sourced from L929 fibroblasts that were grown to confluence in low glucose DMEM supplemented with 10% fetal bovine serum and then serum-starved for 10 days. Medium from the fibroblast cultures was then collected, filter-sterilized and stored at −20°C as L929 conditioned medium. BMDM were seeded at 1×10^6 cells/mL and differentiated using 10% L929 conditioned medium for 5–7 days at 37°C, 5% CO2 on Petri dishes.

Primary monocytes were isolated from heparinized blood of healthy male or female human donors aged 20–35 who provided informed consent, following a protocol approved by the Research Ethics Board of The Hospital for Sick Children. Peripheral blood mononuclear cells were first isolated using Lympholyte-H (Cedarlane). Monocytes were then enriched by negative selection using the EasySep human monocyte isolation kit (StemCell). COS-1 fibroblasts stably expressing the human FcγRIIA receptor were generated and cultured as previously described (Downey et al., 1999). RAW 264.7 cells were cultured as described (Freeman et al., 2016).

METHOD DETAILS

Single-particle labeling and tracking of CD44, Fc receptors and glycomimetics —The ImmunoPure Fab Preparation Kit (Pierce) was used to generate monovalent Fab fragments of anti-CD44, anti-CD32, and anti-CD16/32 antibodies; 2 mg of the monoclonal antibody produced by the IM7, IV.3, and 93 hybridoma cell lines was used as starting material. Fab fragments were directly labeled with the succinimidyl esters of Cy3B or biotin, and the final concentration of the conjugate was determined by Western blotting. Glycomimetics were synthesized as previously described (Paszek et al., 2014). To label single molecules, cells were washed with HBSS (Wisent Bioproducts) then incubated with 10 ng/mL of Cy3B-or biotin-conjugated anti-CD44, antiCD16/32, or 100 ng/mL of anti-HA

clone 3F10 (Roche) Fab fragments for 5 min. For experiments using glycomimetics, 10 nM of the biotinylated 30 nm glycomimetic polymer was first added to cells in PBS at 25°C for 5 min. Cells labeled with biotinylated Fabs or glycomimetics were washed in cold PBS, then incubated with streptavidin-655 Qdots (1:10,000 dilution) for 5 min at 4°C, to minimize lateral mobility and clustering. Cells were subsequently washed with DMEM containing excess biotin to block unoccupied avidin sites and prevent cross-linking. Cells labeled with Cy3B-conjugated Fab fragments were washed in PBS at 25°C. Single cells were then warmed to 37°C and imaged immediately on a Zeiss Axiovert 200M microscope, equipped with a 100× NA 1.45 oil objective, a custom 2.4× magnification lens, and a back-thinned EM-CCD camera (C9100-13, Hamamatsu). Throughout the period of video acquisition, cells were routinely observed and imaged by DIC to ensure they were not retracting. For Qdot-labeled particles, acquisitions were performed at 33 Hz using Volocity software (Perkin-Elmer). For Cy3B-labeled particles, acquisitions were performed at 10 Hz. Single particles labelled with Cy3B were detected and tracked as described (Jaqaman et al., 2008). Unless otherwise indicated, motion types and diffusion coefficients were determined using a moment scaling spectrum (MSS) analysis as previously described (Jaqaman et al., 2011). The dimensions of the confinement zones were derived by eigenvalue decomposition of the variance-covariance matrix of particle positions.

Divide-and-conquer moment scaling spectrum analysis—Where specified, motion types and diffusion coefficients of tracks obtained using Qdots were subjected to a novel transient diffusion analysis method named divide-and-conquer moment scaling spectrum (DC-MSS), described briefly below and in more detail in (Vega, A., Freeman, S., Grinstein, S., & Jaqaman, K., “Multistep track segmentation and motion classification for transient mobility analysis”, manuscript in revision).

Initial segmentation: First, a rolling-window of 11 frames was used to obtain the maximum pairwise distance between track positions within each window along the track, resulting in a maximum pairwise distance time series. After smoothing the time series with a Gaussian kernel (σ: 2 frames) in order to reduce fluctuations resulting from noise, its derivative was taken to find changes in the maximum pairwise distance. The derivative at each time point was then normalized by the pairwise distance value at that time point, so that mobility changes of different scales (e.g. immobile to confined vs. immobile to free) were equally detectable. Points in the normalized derivative time series with absolute values in the top 5% were then taken as boundary points between segments. Because the smoothing Gaussian kernel might blur segment boundaries, short segments with length < 20 frames, making them unclassifiable via MSS (next step), but >= 20−2 σ = 16 frames were extended to 20 frames by shifting the boundary into the adjacent segment, as long as this did not shorten the adjacent segment to < 20 frames. Lastly, because this segmentation scheme tends to over-segment the tracks, the distribution of pairwise distances between all positions in each segment was compared between adjacent segments via a Kolmogorov Smirnov-test, and adjacent segments with a p value > 0.05 were combined.

Segment classification: After the initial segments were found, each segment that was at least 20 frames long was classified using Moment Scaling Spectrum (MSS) analysis (Ferrari

R., 2001; Jaqaman et al., 2011). The thresholds for mobility classification, which depended on track duration, were derived as follows: (i) 10,000 tracks were simulated per track duration (20–500 frames) and per mobility class (tethered, confined, free); (ii) the simulated tracks were analyzed via MSS, generating MSS-value distributions for each mobility class and track duration; and (iii) for each pair of adjacent mobility classes (i.e. tethered vs. confined, and confined vs. free) and track duration, the MSS-value that maximized the ability to distinguish between the two classes (i.e. minimized the classification error on both sides) was taken as the classification threshold.

Post-processing for final segmentation: After classification, any segment that was too short for classification was temporarily merged with an adjacent classified segment, and the combined segment was reclassified. If the combined segment was assigned either the original or a lower mobility classification, the merge was retained. Otherwise, the merge was rejected and the two segments remained separate. This strategy is based on the reasoning that longer observation times should reveal more, not less, confinement. Similarly, adjacent segments with the same classification were temporarily merged with each other and reclassified. If the reclassification resulted in either the original or a lower mobility classification, the merge was retained. Otherwise, these segments were separated, keeping their original classification.

Immunofluorescence—Cells were fixed with 4% PFA (Electron Microscopy Sciences), permeabilized with 0.5% Triton X-100 in PBS, blocked with 5% BSA in PBS, and stained with the indicated antibodies or fluorescent phalloidin in blocking solution (see Extended Methods for reagent details). After staining, coverslips were mounted onto glass slides using ProLong Diamond (Life Technologies).

Transfection—Transfection of RAW cells using FuGeneHD or COS-1 cells using FuGene6 (Promega) was done according to the manufacturer's protocol.

Reagents and plasmids—Where specified, macrophages were preincubated for 10 min in HBSS with 10 μM of either the Arp2/3 complex inhibitor I, CK-666 (Millipore), or the ezrin inhibitor NSC668394 (Millipore) before video recording for single particle tracking, addition of phagocytic targets, or cytoskeletal fractionation. Latrunculin A (Sigma) was used at 1 μM for 510 min. For experiments with suspended cells, the Rho Inhibitor I CT04 and Activator II CN03 (Cytoskeleton) were used at 2.0 μg/mL and incubated for 2 h. For adherent cell experiments, BMDMs were first lifted and incubated with 1.0 μg/mL of Rho Activator II CN03 for 10 min before plating in medium also containing 1.0 μg/mL of CN03 for 3–4 h. Antibodies for immunostaining were used as follows: mouse anti-human FcγRIIA/IV.3 (StemCell Technologies) at 5 μg/mL, Cy3-or Alexa 647-conjugated donkey anti-mouse or anti-human secondary antibodies (Jackson ImmunoResearch) were used at 1 μg/mL. Rhodamine-or Alexa 488-phalloidin (Life Technologies) were used at 1:500. Coverslips were coated with poly-Llysine, mol wt. 70,000–150,000, 0.01% (Sigma) at a 1:10 dilution in PBS at 25°C for 1 h and subsequently coated with a 0.25 mg/mL solution of fluorescein-labelled hyaluronic acid (Sigma) in PBS also at 25°C for 1 h. The Quantikine ELISA Hyaluronan Immunoassay (R&D Systems) was used as per manufacturer's

instructions. Isolation and purification of the hyaluronan binding complex (HABC) from bovine articular cartilage, and its biotinylation was described earlier (Tammi et al., 1994). The labelling of HABC with Alexa 647 is published in (Rilla et al., 2008). The fluorescent HABC was added at 10 μg/ml final concentration in the medium of live cells, and imaged after 5 min. Hyaluronan binding complex was made and used as previously described (Kultti et al., 2006). Alexa 488-or 647-wheat germ agglutinin (Life Technologies) was added to cells at a 1:2000 dilution for 5 min. Hyaluronidase from bovine testes (Sigma) was used at 20 units/mL for 10–30 min at 37 °C in DMEM. LPS from *S. enterica* 595 (Sigma) was used at 500 ng/mL. Ionomycin from *S. conglobatus* (Sigma) was used at 5 μM. Murine CD44wt and CD44ΔCT were subcloned from pBS into the EGFP-C1 vector (Clontech). The transmembrane I actin-binding domain of ezrin (Gowrishankar et al., 2012) was modified to incorporate an HL4.1 (fluorogen-activating protein) with an N-terminal hemagglutinin tag (Schwartz et al., 2015) on the extracellular domain. HAS3-GFP was previously described (Kultti et al., 2006). PLCδ(PH)GFP was previously described (Botelho et al., 2000). FcγRIIA, FcγRIIAΔCT, and FcγRIIA-GFP were generous gifts from Dr. A. D. Schreiber (University of Pennsylvania School of Medicine). Ezrin-GFP was from Stephen Shaw (Addgene plasmid # 20680). Stealth RNAi™ siRNAs (ThermoFisher) were electroporated at 100 pM using a Neon transfection system (ThermoFisher).

Stimulated emission depletion (STED) microscopy—STED was performed using a Leica TCS SP8 STED 3× microscope. Images were acquired using HyD detectors and a 100×/1.4 oil objective. Samples were labeled with Alexa-488 and Cy3-conjugated secondary antibodies and excited at 499 and 554 nm respectively using a white light laser. Emissions were time gated 0.36 ns. Two 1.5 W depletion lasers at 592 and 660 nm were used for the green and red channels, respectively, at 35–56% of maximal power. Images were acquired using Leica LAS X software with a xy pixel size of 31 nm and z step of 200 nm. Acquired images were deconvolved with Huygens Professional software (Scientific Volume Imaging, The Netherlands).

Micropatterning IgG—Micropatterning was performed as described (Freeman et al., 2016). Conformal contact between polydimethylsiloxane stamps that were incubated with 1 mg/mL of human IgG (Sigma) and the glass coverslip was made for 10 s to transfer antibodies. To visualize the IgG, coverslips were stained with 0.1 μg/mL Cy3-conjugated donkey anti-human antibody (Jackson ImmunoResearch) for 5 min.

Particle binding—For opsonisation of erythrocytes, 0.5 mg/mL of rabbit anti-sheep IgG (MP Biomedicals) was incubated at with 200 μL of a 1% solution of washed sheep erythrocytes (MP Biomedicals) for 2 h at 37 °C. For opsonisation, 200 μL of a suspension (1% solids in PBS) of polystyrene beads containing 2% divinylbenzene (1.5, 5, or 8 μm diameter; Bangs Laboratories) was incubated with human IgG (50, 10, or 5 μg/mL; Sigma) for 2 h at 37°C. To assess binding of *Salmonella*, an *S. enterica* serovar typhimurium invasion-defective (ΔinvA) strain of SL1344 expressing an ampicillin-resistance plasmid, pIZ1590, that encodes dsRed was used. ΔinvA SL1344 dsRed *S. enterica* were grown on LB plates containing ampicillin (25 μg/mL) for 24–48 h before inoculating 1 mL of liquid LB with 1 colony and growing at 37°C with aeration for 2–3 h. The bacteria were sedimented

and resuspended in 500 μL of PBS containing either a 1:250 dilution of *Salmonella* O antiserum Group B Factors 1, 4, 5, 12 (BD Biosciences) or a 1:250 dilution of *Salmonella* H antiserum Poly a–z (BD Biosciences). Opsonisation was at room temperature, shaking for 10 min before bacteria were centrifuged, resuspended in PBS, and added to primary macrophages cultured on coverglass. Either equal amounts (1×10^7), or 5×10^8 H-and 1×10^7 O-opsonized bacteria were added to 5×10^5 macrophages for 5–20 min before fixation, as indicated.

Quantification of surface CD44—Adherent macrophages were washed with ice-cold PBS and kept on ice. Cells were subsequently incubated with saturating concentrations (20 μg/mL) of biotinylated anti-CD44 Fab fragments for 10 min on ice to prevent endocytosis. Cells were then washed three times with cold PBS before extraction with lysis buffer (150 mM sodium chloride, 1% NP-40, 0.5% sodium deoxycholate, 0.1% SDS, 50 mM Tris, pH 8.0). Sample buffer containing 10% 2-mercaptoethanol was added to lysates or known quantities of fab fragments before separation by PAGE under reducing conditions. Immunoblotting was performed with streptavidin-HRP (Cell Signaling Technology) or mouse anti-β-actin (Abcam, clone AC-15).

Cytoskeletal fractionation—Cells were incubated for 1 min with cytoskeletal stabilizing buffer (4 M glycerol, 25 mM Pipes pH 6.9, 1 mM EGTA, 1 mM MgCl2) and 0.1% Triton-X followed by centrifugation for 5 min at 7,500g at 4°C. The pellet, representing the Triton-insoluble cytoskeletal fraction, was resuspended with the same buffer. Supernatant (S) and pellet (P) were separated under reducing conditions and analyzed by immunoblotting. Antibody binding was detected by chemiluminescence (Amersham ECL prime, GE Healthcare) on an Odyssey FC Imaging System (LI-COR) equipped with Image Studio Software (Li-COR). The following antibodies were used: rat anti-CD44 (Hybridoma Bank, University of Iowa, clone 5D2-27), mouse anti-β-actin (Abcam, clone AC-15), rabbit anti-CD32 (Santa Cruz, sc-28842) and goat anti-ezrin (Santa Cruz, C-19) with appropriate secondary antibodies conjugated to HRP (Jackson ImmunoResearch).

Confocal microscopy and image analysis—Unless otherwise indicated, imaging was performed using a Quorum spinning disc mounted on a Zeiss Axiovert 200M microscope, using 63× or 100× oil objectives, a 1.5× magnification lens, and a back-thinned EM-CCD camera (C9100-13, Hamamatsu). Acquisitions were controlled by the Volocity software (Perkin-Elmer), exported and processed with MatLab (MathWorks) for single-particle tracking, or analyzed and quantified using Volocity or Image J (NIH) software.

QUANTIFICATION AND STATISTICAL ANALYSIS

The number of experiments and cells quantified are indicated in the individual Figure Legends. Each experiment (n) was performed with cells from different animals or human donors. The Mann-Whitney test was used to determine p values between populations of single cell measurements. Otherwise, student t-tests or two-way ANOVA tests were used to compare sets of matched samples.

DATA AND SOFTWARE AVAILABILITY

The Divide and Conquer-Moment Scaling Spectrum software has been made available and can be found using the following link: http://www.utsouthwestern.edu/labs/jaqaman/software. The u-Track software can be found here: http://www.utsouthwestern.edu/labs/danuser/software.

KEY RESOURCES TABLE

REAGENT or RESOURCE	SOURCE	IDENTIFIER
Antibodies		
anti-β-actin (clone AC-15)	Abcam	Cat. # ab6276
anti-CD16/32 (rat, clone 93)	BioLegend	Cat. # 101302
anti-CD32 (mouse, clone IV.3)	StemCell Technologies	Cat. # 60012
anti-CD32 (rabbit)	Santa Cruz	Cat. # sc-28842
anti-CD44 (rat, clone 5D2-27)	Developmental Studies Hybridoma Bank, University of Iowa	5D2-27
anti-CD44 (rat, clone IM7)	StemCell Technologies	Cat. # 60068
anti-ezrin C-19 (goat)	Santa Cruz	Cat. # sc-6407
anti-HA-biotin, high affinity (clone 3F10)	Millipore Sigma	Cat. # 1258167001
IgG from human serum	Millipore Sigma	Cat. # I4506
Salmonella O antiserum Group B Factors 1,4,5,12	BD Biosciences	Cat. # 229481
Salmonella H antiserum Poly a–z	BD Biosciences	Cat. # 224061
anti-sheep red blood cell (rabbit)	MP Biomedicals	Cat. # 0855806
Streptavidin-HRP	Cell Signaling Technology	Cat. # 3999
Bacterial and Virus Strains		
S. enerica SL1344ΔinvA + pIZ1590	Segura et al., 2004	N/A
Chemicals, Peptides, and Recombinant Proteins		
Arp2/3 inhibitor CK-666	Millipore Sigma	Cat. # SML0006
Ezrin inhibitor NSC668394	Millipore Sigma	Cat. # 341216
Glycomimetic-biotinylated	This paper	N/A
Hyaluronan binding complex-Alexa 647	Rilla et al., 2008	N/A
Hyaluronan binding complex-biotinylated	Tammi et al., 1994	N/A
Hyaluronidase from bovine testes Type I-S	Millipore Sigma	Cat. # H3506
Ionomycin from *S. conglobatus*	Millipore Sigma	Cat. # I9657
LPS from *S. enterica* 595	Millipore Sigma	Cat. # L9764
Phalloidin-Alexa 488	ThermoFisher	Cat. # A12379
Phalloidin-Rhodamine	ThermoFisher	Cat. # R415
Poly-L-Lysine solution	Millipore Sigma	Cat. # P8920
Polystyrene beads containing 2% divinylbenzene (1.5, 5, 8 μm diameter)	Bangs Laboratories	Cat. Code PS02N
Rho Inhibitor I CT04	Cytoskeleton	Cat. # CT04

REAGENT or RESOURCE	SOURCE	IDENTIFIER
Rho Activator II CN03	Cytoskeleton	Cat. # CN03
Wheat germ agglutinin-Alexa 488	ThermoFisher	Cat. # W11261
Wheat germ agglutinin-Alexa 647	ThermoFisher	Cat. # W32466
Critical Commercial Assays		
EasySep human monocyte isolation kit	StemCell	Cat. # 19359
Quantikine ELISA Hyaluronan Immunoassay	R&D Systems	Cat. # DHYALO
ImmunoPure Fab Preparation Kit	Pierce	Cat. # 44985
Experimental Models: Cell Lines		
COS-1 fibroblasts	ATCC	ATCC: CRL-1650
L-929 fibroblasts	ATCC	ATCC: CCL-1
RAW 264.7 cells	ATCC	ATCC: TIB-71
Experimental Models: Organisms/Strains		
Mouse: C57Bl/6 wildtype	The Jackson Laboratory	JAX: 000664
Mouse: B6.129(Cg)-Cd44^{tm1Hbg}/JCD44$^{-/-}$	The Jackson Laboratory	JAX: 005085
Oligonucleotides		
CD44 siRNA	ThermoFisher	Cd44MSS273566 Cat No./Lot No. 10620318 – 341909 E07
Recombinant DNA		
Ezrin-GFP	Addgene	# 20680
FcγRIIA	Downey et al., 1999	N/A
FcγRIIA-GFP	Booth et al., 2002	N/A
FcγRIIAΔCT-GFP	This paper	N/A
Hyaluronan Synthase 3-GFP	Kultti et al., 2006	N/A
Murine CD44wt-GFP	This paper	N/A
Murine CD44ΔCT-GFP	This paper	N/A
N-terminal HA-tagged transmembrane actin-binding domain (ezrin)	This paper	N/A
N-terminal HA-tagged transmembrane actin-binding domain (ezrin) R579A	This paper	N/A
Software and Algorithms		
Divide and Conquer-Moment Scaling Spectrum	This paper	http://www.utsouthwestern.edu/labs/jaqaman/software
MatLab	MathWorks	www.mathworks.com/products/matlab.html
u-Track	Jaqaman et al., 2008	http://www.utsouthwestern.edu/labs/danuser/software
Volocity	PerkinElmer	http://cellularimaging.perkinelmer.com/

Supplementary Material

Refer to Web version on PubMed Central for supplementary material.

Acknowledgments

We thank Dr. C. Valley for cloning of the HA-tagged transmembrane actin binding proteins. SAF is supported by a Banting fellowship of the Canadian Institutes of Health Research (CIHR). AV is supported by a CPRIT training grant RP140110. DSL and SM were supported by the Human Frontiers Science Program (Grant RGP0027/2012). MT is supported by the Sigrid Juselius Foundation, and the Cancer Center of Eastern Finland. JP was supported by NSERC. KJ is supported by NIH/NIGMS MIRA R35GM119619, CPRIT recruitment award R1216, and by the UTSW Endowed Scholars Program. SG is supported by grant FDN-143202 from the CIHR.

References

Aruffo A, Stamenkovic I, Melnick M, Underhill CB, Seed B. CD44 is the principal cell surface receptor for hyaluronate. Cell. 1990; 61:1303–1313. [PubMed: 1694723]

Botelho RJ, Teruel M, Dierckman R, Anderson R, Wells A, York JD, Meyer T, Grinstein S. Localized biphasic changes in phosphatidylinositol-4,5-bisphosphate at sites of phagocytosis. The Journal of cell biology. 2000; 151:1353–1368. [PubMed: 11134066]

Chang MY, Tanino Y, Vidova V, Kinsella MG, Chan CK, Johnson PY, Wight TN, Frevert CW. A rapid increase in macrophage-derived versican and hyaluronan in infectious lung disease. Matrix biology : journal of the International Society for Matrix Biology. 2014; 34:1–12. [PubMed: 24472738]

Chen Y, Veracini L, Benistant C, Jacobson K. The transmembrane protein CBP plays a role in transiently anchoring small clusters of Thy-1, a GPI-anchored protein, to the cytoskeleton. Journal of cell science. 2009; 122:3966–3972. [PubMed: 19825940]

Downey GP, Botelho RJ, Butler JR, Moltyaner Y, Chien P, Schreiber AD, Grinstein S. Phagosomal maturation, acidification, and inhibition of bacterial growth in nonphagocytic cells transfected with FcgammaRIIA receptors. The Journal of biological chemistry. 1999; 274:28436–28444. [PubMed: 10497205]

Faure S, Salazar-Fontana LI, Semichon M, Tybulewicz VL, Bismuth G, Trautmann A, Germain RN, Delon J. ERM proteins regulate cytoskeleton relaxation promoting T cell-APC conjugation. Nature immunology. 2004; 5:272–279. [PubMed: 14758359]

Fehon RG, McClatchey AI, Bretscher A. Organizing the cell cortex: the role of ERM proteins. Nature reviews Molecular cell biology. 2010; 11:276–287. [PubMed: 20308985]

Ferrari R, M AJ, Young WR. Strongly and weakly self-similar diffusion. Physica D. 2001; 154:111–137.

Freeman SA, Goyette J, Furuya W, Woods EC, Bertozzi CR, Bergmeier W, Hinz B, van der Merwe PA, Das R, Grinstein S. Integrins Form an Expanding Diffusional Barrier that Coordinates Phagocytosis. Cell. 2016; 164:128–140. [PubMed: 26771488]

Fujiwara T, Ritchie K, Murakoshi H, Jacobson K, Kusumi A. Phospholipids undergo hop diffusion in compartmentalized cell membrane. Journal of Cell Biology. 2002; 157:1071–1081. [PubMed: 12058021]

Ghosh M, Song X, Mouneimne G, Sidani M, Lawrence DS, Condeelis JS. Cofilin promotes actin polymerization and defines the direction of cell motility. Science. 2004; 304:743–746. [PubMed: 15118165]

Gowrishankar K, Ghosh S, Saha S, C R, Mayor S, Rao M. Active remodeling of cortical actin regulates spatiotemporal organization of cell surface molecules. Cell. 2012; 149:1353–1367. [PubMed: 22682254]

Haggie PM, Kim JK, Lukacs GL, Verkman AS. Tracking of quantum dot-labeled CFTR shows near immobilization by C-terminal PDZ interactions. Molecular biology of the cell. 2006; 17:4937–4945. [PubMed: 16987954]

Jaqaman K, Kuwata H, Touret N, Collins R, Trimble WS, Danuser G, Grinstein S. Cytoskeletal control of CD36 diffusion promotes its receptor and signaling function. Cell. 2011; 146:593–606. [PubMed: 21854984]

Jaqaman K, Loerke D, Mettlen M, Kuwata H, Grinstein S, Schmid SL, Danuser G. Robust single-particle tracking in live-cell time-lapse sequences. Nat Methods. 2008; 5:695–702. [PubMed: 18641657]

Kalay Z, Fujiwara TK, Otaka A, Kusumi A. Lateral diffusion in a discrete fluid membrane with immobile particles. Physical review E, Statistical, nonlinear, and soft matter physics. 2014; 89:022724.

Kultti A, Rilla K, Tiihonen R, Spicer AP, Tammi RH, Tammi MI. Hyaluronan synthesis induces microvillus-like cell surface protrusions. The Journal of biological chemistry. 2006; 281:15821–15828. [PubMed: 16595683]

Kusumi A, Fujiwara TK, Chadda R, Xie M, Tsunoyama TA, Kalay Z, Kasai RS, Suzuki KG. Dynamic organizing principles of the plasma membrane that regulate signal transduction: commemorating the fortieth anniversary of Singer and Nicolson's fluid-mosaic model. Annual review of cell and developmental biology. 2012; 28:215–250.

Kusumi A, Sako Y. Cell surface organization by the membrane skeleton. Current opinion in cell biology. 1996; 8:566–574. [PubMed: 8791449]

Lammermann T, Bader BL, Monkley SJ, Worbs T, Wedlich-Soldner R, Hirsch K, Keller M, Forster R, Critchley DR, Fassler R, et al. Rapid leukocyte migration by integrin-independent flowing and squeezing. Nature. 2008; 453:51–55. [PubMed: 18451854]

Laurent TC, Fraser JR. Hyaluronan. FASEB journal : official publication of the Federation of American Societies for Experimental Biology. 1992; 6:2397–2404. [PubMed: 1563592]

Lee-Sayer SS, Dong Y, Arif AA, Olsson M, Brown KL, Johnson P. The where, when, how, and why of hyaluronan binding by immune cells. Frontiers in immunology. 2015; 6:150. [PubMed: 25926830]

Lesley J, Hascall VC, Tammi M, Hyman R. Hyaluronan binding by cell surface CD44. Journal of biological chemistry. 2000; 275:26967–75. [PubMed: 10871609]

Lomakin AJ, Lee KC, Han SJ, Bui DA, Davidson M, Mogilner A, Danuser G. Competition for actin between two distinct F-actin networks defines a bistable switch for cell polarization. Nature cell biology. 2015; 17:1435–1445. [PubMed: 26414403]

Masters TA, Pontes B, Viasnoff V, Li Y, Gauthier NC. Plasma membrane tension orchestrates membrane trafficking, cytoskeletal remodeling, and biochemical signaling during phagocytosis. Proceedings of the National Academy of Sciences of the United States of America. 2013; 110:11875–11880. [PubMed: 23821745]

Morone N, Fujiwara T, Murase K, Kasai RS, Ike H, Yuasa S, Usukura J, Kusumi A. Three-dimensional reconstruction of the membrane skeleton at the plasma membrane interface by electron tomography. The Journal of cell biology. 2006; 174:851–862. [PubMed: 16954349]

Nakada C, Ritchie K, Oba Y, Nakamura M, Hotta Y, Iino R, Kasai RS, Yamaguchi K, Fujiwara T, Kusumi A. Accumulation of anchored proteins forms membrane diffusion barriers during neuronal polarization. Nature cell biology. 2003; 5:626–632. [PubMed: 12819789]

Paszek MJ, DuFort CC, Rossier O, Bainer R, Mouw JK, Godula K, Hudak JE, Lakins JN, Wijekoon AC, Cassereau L, et al. The cancer glycocalyx mechanically primes integrin-mediated growth and survival. Nature. 2014; 511:319–325. [PubMed: 25030168]

Pienimaki JP, Rilla K, Fulop C, Sironen RK, Karvinen S, Pasonen S, Lammi MJ, Tammi R, Hascall VC, Tammi MI. Epidermal growth factor activates hyaluronan synthase 2 in epidermal keratinocytes and increases pericellular and intracellular hyaluronan. Journal of biological chemistry. 2001; 276:20428–35. [PubMed: 11262389]

Rilla K, Tiihonen R, Kultti A, Tammi M, Tammi R. Pericellular hyaluronan coat visualized in live cells with a fluorescent probe is scaffolded by plasma membrane protrusions. The journal of histochemistry and cytochemistry : official journal of the Histochemistry Society. 2008; 56:901–910. [PubMed: 18574248]

Saha S, Lee IH, Polley A, Groves JT, Rao M, Mayor S. Diffusion of GPI-anchored proteins is influenced by the activity of dynamic cortical actin. Molecular biology of the cell. 2015; 26:4033–4045. [PubMed: 26378258]

Schwartz SL, Yan Q, Telmer CA, Lidke KA, Bruchez MP, Lidke DS. Fluorogen-activating proteins provide tunable labeling densities for tracking FcepsilonRI independent of IgE. ACS chemical biology. 2015; 10:539–546. [PubMed: 25343439]

Serrador JM, Nieto M, Alonso-Lebrero JL, del Pozo MA, Calvo J, Furthmayr H, Schwartz-Albiez R, Lozano F, Gonzalez-Amaro R, Sanchez-Mateos P, et al. CD43 interacts with moesin and ezrin and

regulates its redistribution to the uropods of T lymphocytes at the cell-cell contacts. Blood. 1998; 91:4632–4644. [PubMed: 9616160]

Singer SJ, Nicolson GL. The fluid mosaic model of the structure of cell membranes. Science. 1972; 175:720–731. [PubMed: 4333397]

Tammi R, Agren UM, Tuhkanen AL, Tammi M. Hyaluronan metabolism in skin. Progress in histochemistry and cytochemistry. 1994; 29:1–81.

Trimble WS, Grinstein S. Barriers to the free diffusion of proteins and lipids in the plasma membrane. The Journal of cell biology. 2015; 208:259–271. [PubMed: 25646084]

HIGHLIGHTS

- CD44 functions as a picket, affixing the cortical actin cytoskeleton to the membrane -the extracellular domain of CD44 binds hyaluronan, which forms a pericellular coat
- the picket fence and pericellular coat limit the mobility of phagocytic receptors
- remodeling of the actin fence enables receptors to cluster and initiate phagocytosis

The actin cytoskeleton is affixed to the plasma membrane by a cell surface protein bound to extracellular matrix forming a barrier that limits receptor mobility

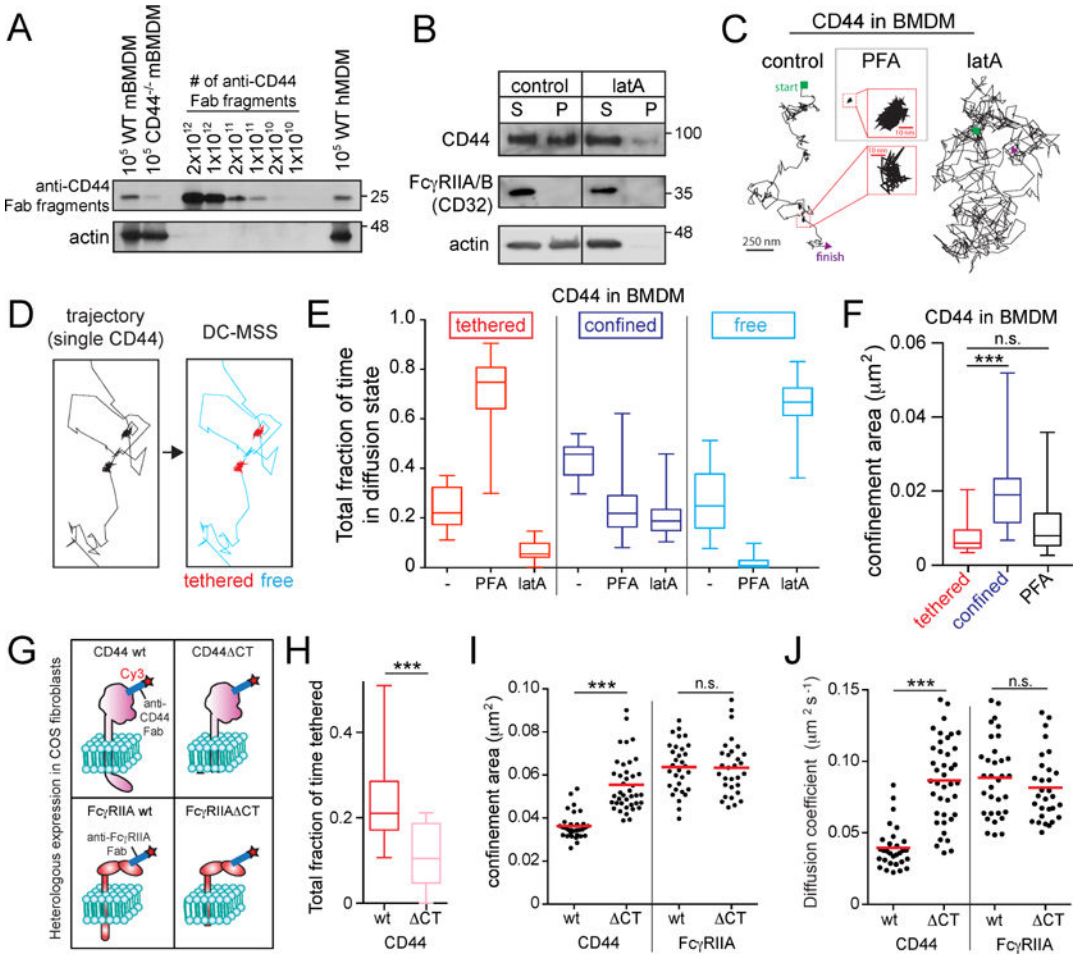

Figure 1. CD44 undergoes “stop-and-go” motion by tethering to the submembrane cytoskeleton

A) Murine bone marrow-derived macrophages (mBMDM) or human monocyte-derived macrophages (hMDM) were incubated with saturating amounts of biotinylated anti-CD44 Fab, subjected to electrophoresis and blotting, and compared to known quantities of Fab. Actin used as loading control. **B)** BMDM were untreated (control) or treated with 1 μM latrunculin A (latA) for 5 min, extracted in actin-stabilizing buffer and centrifuged. Pellet (P) and supernatant (S) analyzed by immunoblotting. Representative of 5 experiments. **C)** Single CD44 particles were visualized on the dorsal side of BMDMs using anti-CD44 Fab labeled with Qdots and tracked for 30 s at 33 Hz under control conditions, or following treatment with LatA (5 min) or PFA (10 min). **D–F)** Trajectories were analyzed using DC-MSS, that recognized segments of trajectories as tethered (red), confined-mobile (blue), or free (cyan). *See also* supplementary Figure 1. **E)** Fraction of time CD44 displays each motion type, determined for >25 cells recorded for 30 s at 33 Hz from 3 experiments. Here and elsewhere boxplots represent pooled distribution of single cells, illustrating the median (central line), interquartile ranges (lower and upper regions of box), and full range (whiskers). **F)** CD44 confinement area determined using DC-MSS. **G–J)** Full-length CD44 (wt), CD44 with its cytoplasmic tail deleted (CD44ΔCT), FcγRIIA wt or FcγRIIAΔCT were heterologously expressed in COS-1 cells. Single CD44 or FcγRIIA particles visualized using Fab labeled with Qdots (H) or Cy3B (I–J, shown diagrammatically in G). **H)** Fraction

of time spent in tethered mode by CD44wt and CD44ΔCT. **I)** Confinement area of CD44 or FcγRIIA determined by traditional MSS for >30 cells recorded 5 s at 10 Hz from 3 experiments. Here and elsewhere dots represent the median for each cell, while horizontal line is the overall mean. **J)** Diffusion coefficient determined for the same recordings as in (H).

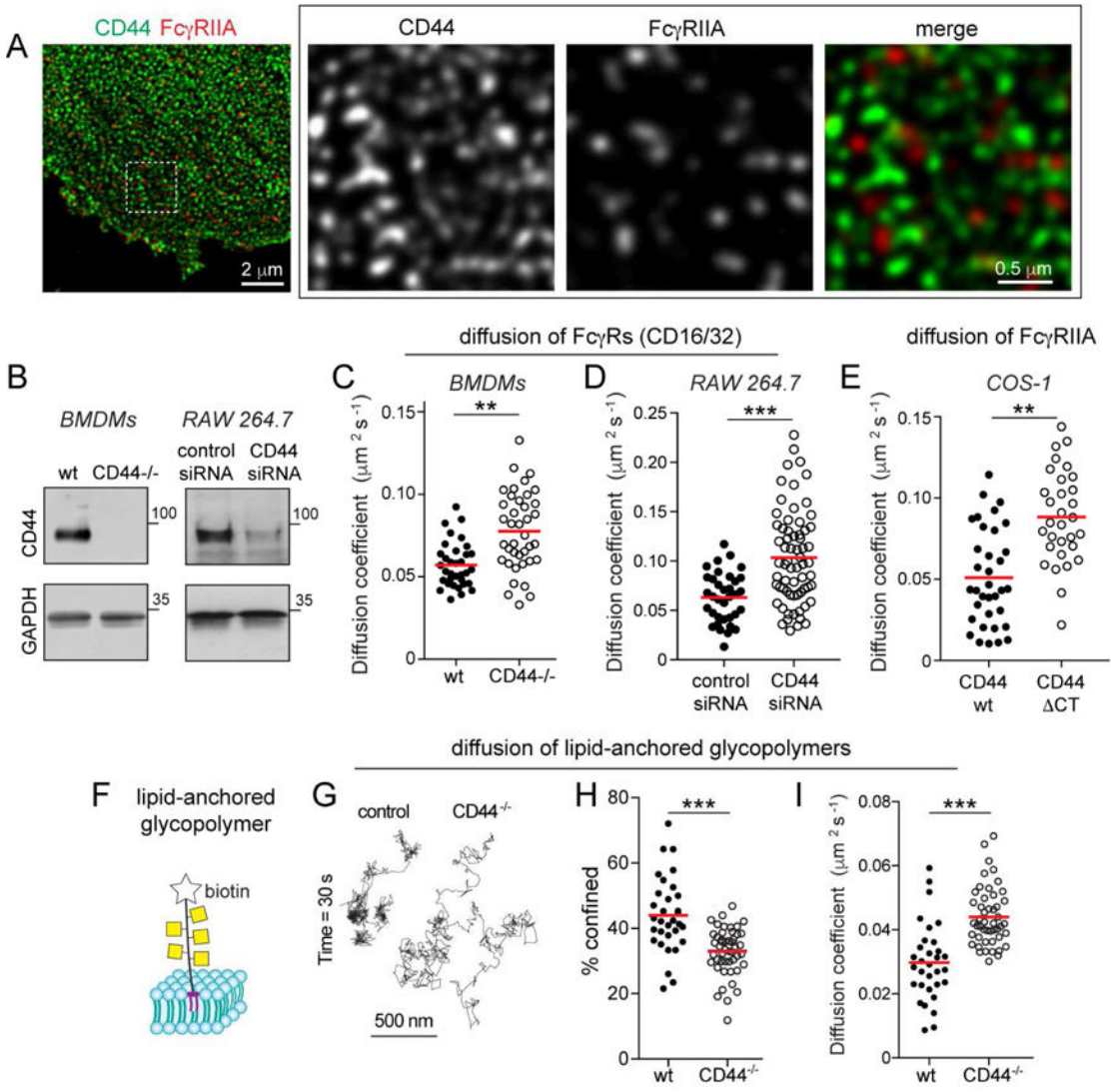

Figure 2. CD44 curtails diffusion of Fcγ receptors and lipid anchored glycopolymers

A) Human macrophages stained for CD44 (green) and FcγRIIA (red) and imaged by STED. **B)** CD44 expression in wildtype or CD44$^{-/-}$BMDM, or RAW macrophages. **C–D)** Comparison of diffusion coefficient of Fcγ receptors in wt or CD44$^{-/-}$BMDM, or RAW cells treated with scrambled or CD44 siRNA (D). Fcγ receptors labelled with Cy3B-tagged Fab and tracked over 5 s at 10 Hz. Median diffusion coefficients determined for >30 cells from 3 experiments. **E)** Diffusion coefficient of Fcγ receptors in COS-1 cells transfected with full-length (wt) or truncated (ΔCT) CD44. **F)** Schematic of synthetic glycopolymer used in panels C–E. It consists of repeating units of N-acetyl galactosamine, is labelled with biotin and inserts into the outer leaflet of the membrane via a dipalmitoyl terminus. **G–I)** Qdots were affixed to single glycopolymers and their motion tracked in wt and CD44$^{-/-}$BMDMs over 30 s at 33 Hz. **G)** Representative trajectories. **H)** Fraction of particles undergoing confined diffusion for >30 cells from 3 experiments. **I)** Median diffusion coefficients for the recordings in (D).

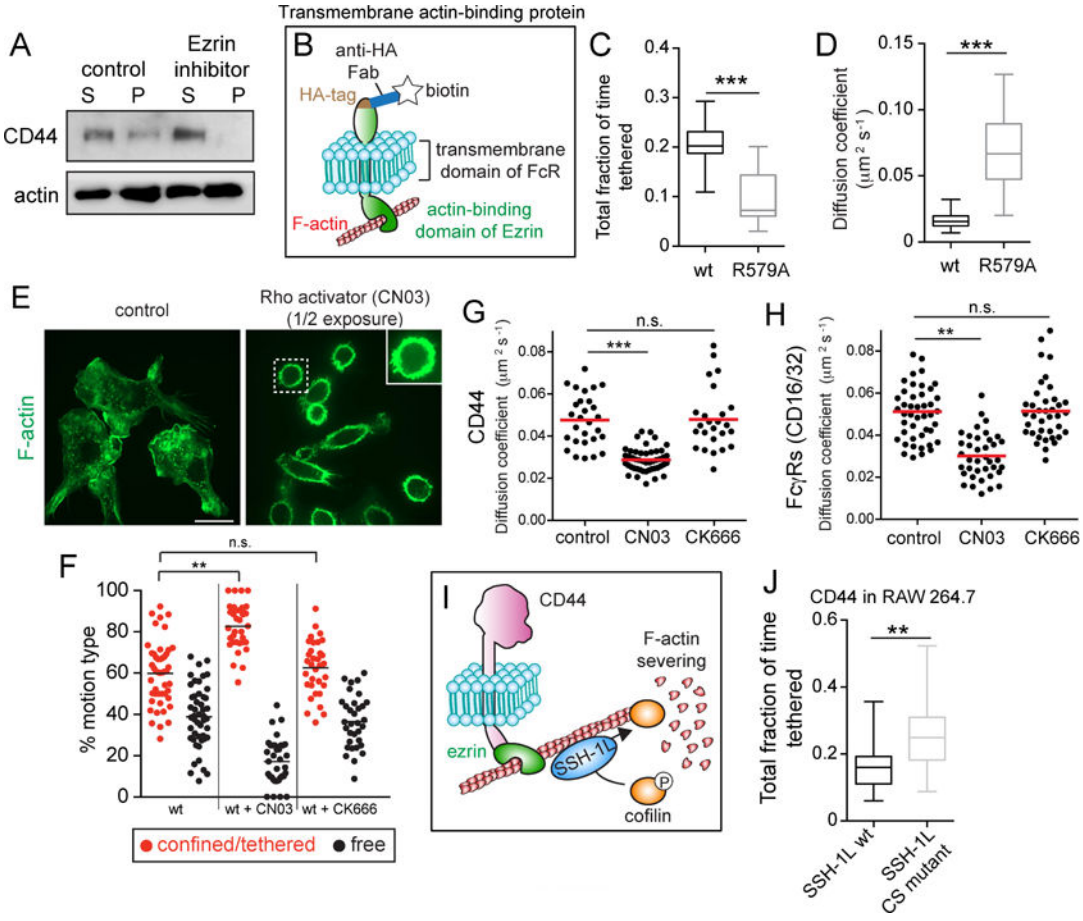

Figure 3. The actin-binding domain of ezrin is necessary and sufficient to tether CD44, which is released by cofilin-mediated severing of actin filaments

A) BMDMs treated with or without 10 μM of ezrin inhibitor NSC668394 were extracted in actin-stabilizing buffer and centrifuged. Pellet (P) and supernatant (S) were analyzed by immunoblotting. Representative of 3 experiments. **B)** Schematic of the construct used in C,D and F. A transmembrane actin-binding protein was engineered by fusing the actin-binding domain of ezrin to the transmembrane domain of Fc receptor, tagged with hemagglutinin (HA) used to attach biotinylated anti-HA Fab for single-particle tracking. An otherwise identical construct bearing a R579A mutation was used as an inactive control. **C)** Fraction of time spent tethered by the unmodified (wt) and mutant (R579A) constructs, determined for >25 cells from 3 experiments. **D)** Diffusion coefficient estimates for the recordings in I. **E)** BMDMs treated with or without Rho activator (CN03) were fixed and stained for F-actin. Right panel image was acquired using ½ the exposure time used for the left; exposure time for inset in right panel was same as for the left panel. **F)** Cells expressing the actin-binding chimera were treated with 1.0 μg/mL CN03 for 2–3 h or 10 μM CK666 for 20 min. Fraction of time spent undergoing restricted or free motion determined for >35 cells from 3 experiments. Tethered and confined modes were not separated. **G–H)** BMDMs were treated with CN03 or CK666 as above before labeling single particles with Cy3-labeled Fab against CD44 or FcγRs. Particles tracked for 10 s at 10 Hz and median diffusion coefficients for >25 cells from 3 experiments are plotted for CD44 (G) and FcγRs (H). **I)** Schematic

illustrating the regulation of actin filament stability by cofilin. Slingshot (SSH-1L) localizes to actin filaments and dephosphorylates cofilin to enable its binding and severing of the filament. **J)** CD44 mobility assessed in RAW cells transfected with wt or phosphatase-dead (CS) SSH-1L. Single CD44 molecules visualized using Qdots tracked for 30 s at 33 Hz and the fraction of time spent in the tethered state calculated for >25 cells from 3 experiments.

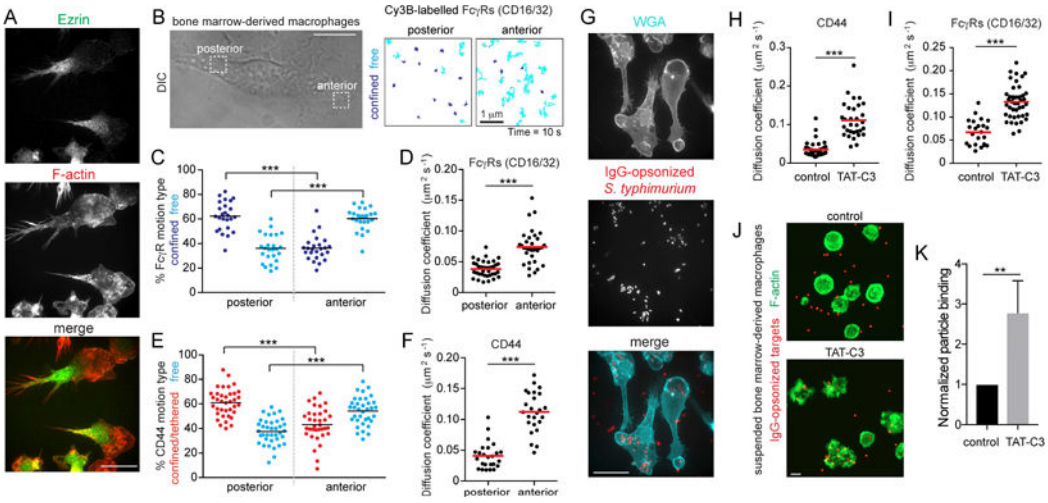

Figure 4. Polarization of cytoskeletal networks orchestrates picket and receptor diffusion

A) BMDMs fixed and stained for ezrin (top) and F-actin (middle); merged images at bottom. Bar = 40 μm. **B)** Polarized BMDMs were selected to visualize CD44 or FcγRs with Cy3B-labelled Fab. Particles tracked for 10 s at 10 Hz at the front and back of the cell. Scale bar = 10 μm. Trajectories are color-coded as confined/tethered (blue) or free (cyan). **C–F)** Motion type (C and E) and diffusion coefficient (D and F) of FcγRs (C–D) or CD44 (E–F) determined for >25 cells from 3 experiments. **G)** BMDMs were challenged with ΔinvA *S. typhimurium* expressing dsRed and opsonized against O-antigens for 5 min and stained with wheat-germ agglutinin (WGA, cyan). **H–I)** BMDMs were treated with the Rho inhibitor (TAT-C3) before single-particle tracking for 10 s at 10 Hz; diffusion coefficient of CD44 (H) or FcγRs (I) was determined for >23 cells from 3 experiments. **J–K)** BMDMs treated in suspension with TAT-C3 for 2 h before challenge with 1.5 μm IgG-opsonized latex beads (red). Cells were fixed and stained for F-actin (green; panel J). Bar = 10 μm. Particle binding presented as means ± SE of >15 fields containing >5 cells each from 3 experiments (K).

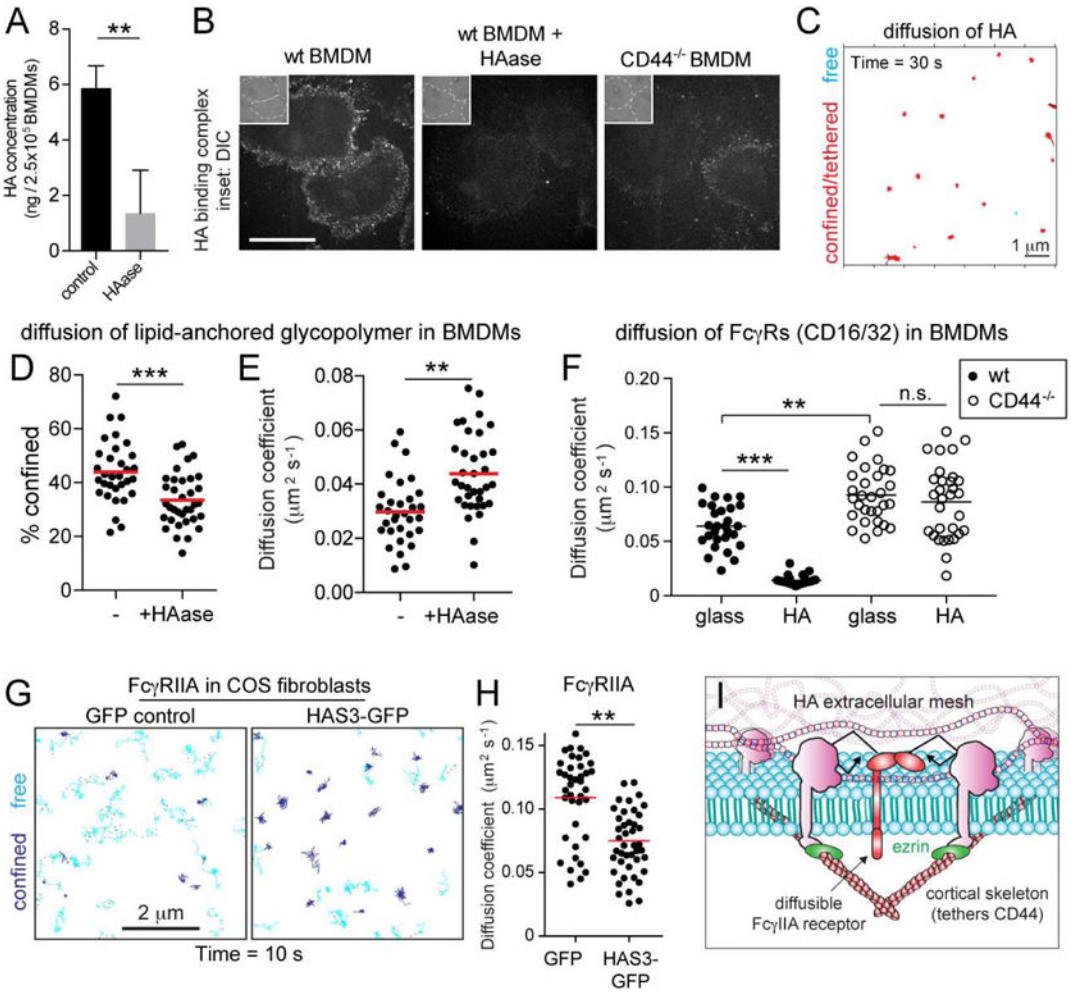

Figure 5. An immobile pericellular exoskeleton of hyaluronan (HA) curtails diffusion of membrane-associated molecules

A) The concentration of HA was determined by ELISA for control and HAase-treated (20 units/mL, 30 min at 37°C) BMDM extracts. Means ± SE of 3 determinations. **B)** Wildtype and CD44$^{-/-}$BMDMs were treated as indicated before incubation with fluorescent HA-binding complex and imaging. Insets are DIC. Bar = 40 μm. **C)** BMDMs incubated with biotinylated HA-binding protein, followed by streptavidin Qdots that were tracked for 30 s at 33 Hz. Representative trajectories shown. **D–E)** Qdots were affixed to biotinylated glycopolymers and their motion tracked in control and HAase-treated BMDMs over 30 s at 33 Hz. Percent confinement I and median diffusion coefficient (F) of >30 cells from 3 experiments. **F)** Fcγ receptors visualized with Cy3B-labelled Fab in HAase-treated BMDMs seeded on glass or HA-coated glass. Receptors were tracked in the ventral surface of cells over 10 s at 10 Hz and median diffusion coefficient determined for >25 cells from 3 experiments. **GH)** COS-1 cells expressing FcγRIIA were transfected with GFP or HA synthase 3 (HAS3)-GFP and receptors visualized with Cy3B-labelled Fab. Receptors were tracked over 10 s at 10 Hz. Representative trajectories (G), where blue indicates confinement and cyan free motion; median diffusion coefficients determined for >30 cells from 3

experiments shown in (H). **I)** Model illustrating proposed mechanism whereby HA restricts receptor diffusion.

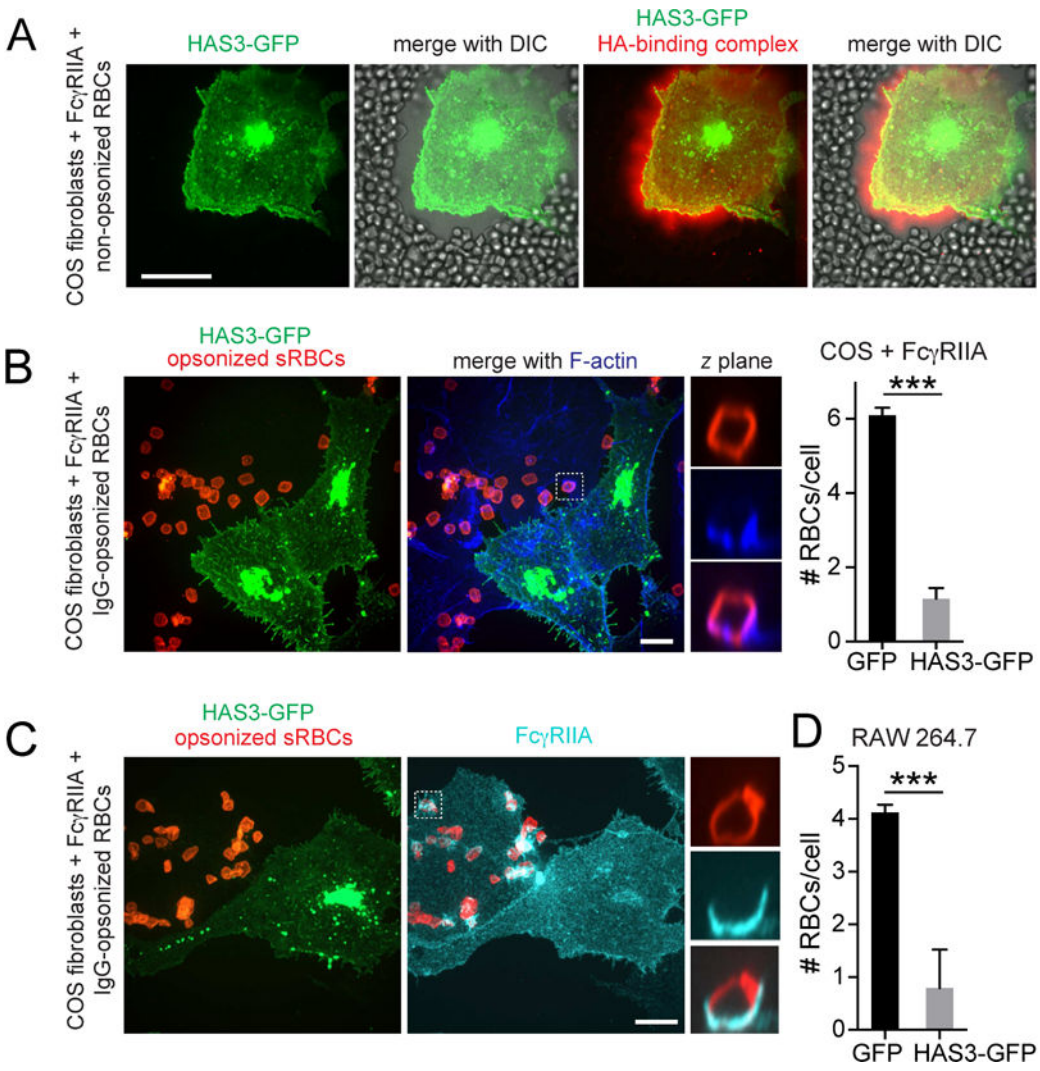

Figure 6. Hyaluronan generated by HAS3 establishes a barrier to receptor access and particle binding

A) HA was visualized in COS-1 cells transfected with HAS3-GFP using fluorescent HA-binding complex (red) before addition of red blood cells, apparent by DIC. **B)** COS-1 cells expressing FcγRIIA were transfected with HAS3-GFP (green) and incubated with IgG-opsonized RBCs (red, *left*). Phalloidin staining (blue). Graph shows the number of RBCs associated to COS-1 cells transfected with GFP or HAS3-GFP. Means ± SE of 50 cells from 3 experiments. Total number of RBCs associated (i.e. bound plus internalized; #RBCs) is shown. **C)** COS-1 cells expressing FcγRIIA were transfected with HAS3-GFP (green) and incubated with RBCs, followed by FcγRIIA staining (cyan). **D)** Quantification of RBCs associated to RAW 264.7 cells transfected with GFP or HAS3-GFP. Means ± SE of 50 cells from 3 experiments.

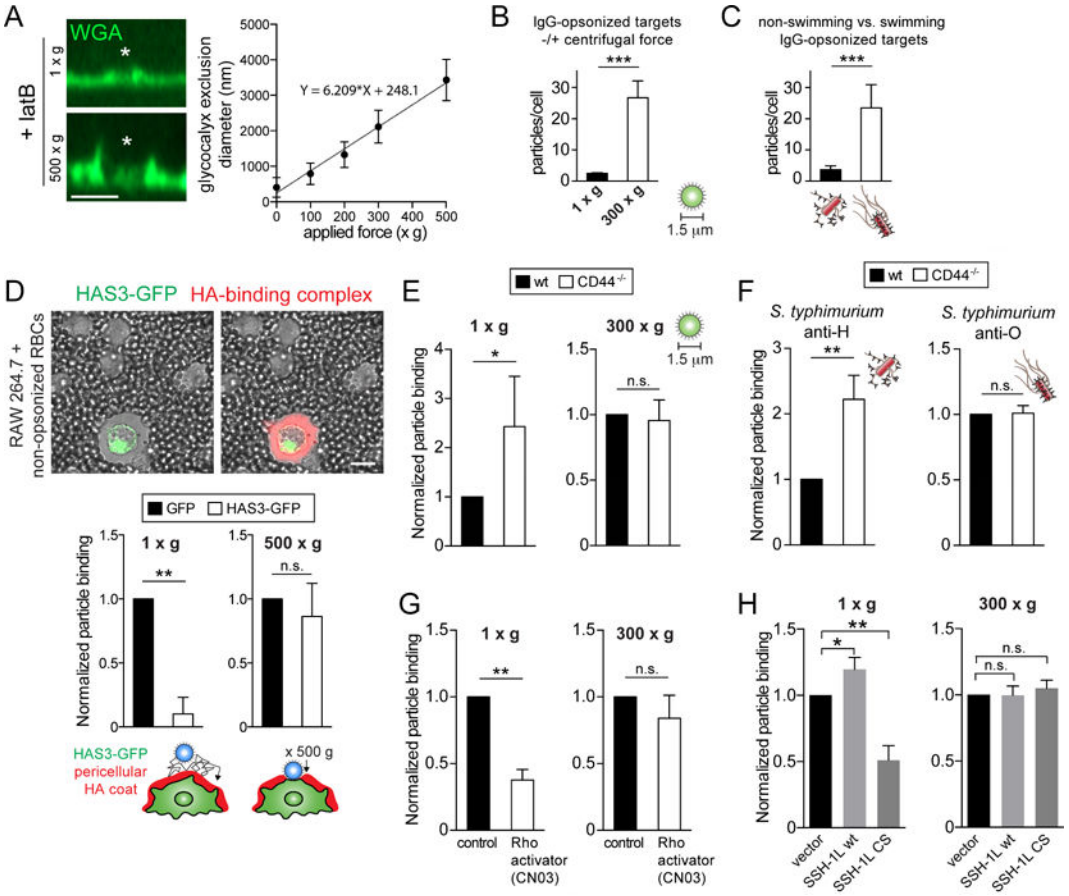

Figure 7. The CD44-structured picket-fence is overcome by force exerted by phagocytic targets

A) Control or LatA-treated BMDMs were exposed to 5 μm beads (asterisks = centre of bead) with or without application of centrifugal force (100–500 xg for 1 min). Glycocalyx exclusion was visualized with WGA (green) and is plotted on the right as a function of centrifugal force. Means ± SE from >100 contacts per condition, from 3 experiments. **B)** BMDMs challenged with 1.5 μm IgG-opsonized beads in the absence or presence of applied *g* force (300 xg). The number of beads bound per cell was determined, shown as means ± SE of 5 determinations. **C)** BMDMs were challenged for 20 min with equal amounts of dsRed-expressing ΔinvA *S. typhimurium* opsonized against H-(flagella) or O-(LPS) antigens. Anti-H greatly reduces the ability of the bacteria to swim (Supplementary Video 3). Number of bacteria bound per cell is shown as means ± SE of 5 determinations. **D)** RAW cells transiently transfected with HAS3-GFP stained for HA with a fluorescent HA-binding complex (red) and incubated with non-opsonized RBCs to visualize the exclusion area by DIC (left). Similarly transfected cells challenged with 8 μm opsonized beads in the absence or presence of applied centrifugal force. Number of beads bound per cell is shown as means ± SE of 3 determinations**. E–F)** Wildtype and $CD44^{-/-}$BMDMs challenged with beads or ΔinvA *S. typhimurium* (F) as in B–C. **G–H)** Control or CN03-treated BMDMs (G) or RAW cells expressing a control vector, wildtype Slingshot (SSH-1L) or phosphatase-dead

Slingshot (SSH-1L CS) (H) were challenged as in B. Particle binding presented as means ± SE of >50 cells from 3 experiments.